Cureus Journal of Engineering

Open Access Original Article

Polyaniline: Robust Green Light-Driven Photocatalyst for Multi-Textile Dye Degradation

Bhagwan Daphal [1] , Vivekanand S. Jawale [1] , Vikram Pandit [2] , Vrishali Edlabadkar [3]

1. Department of Chemistry, Progressive Education Society's Modern College of Engineering, Pune, IND 2. Department of Chemistry, Haribhai V. Desai College, Pune, IND 3. Department of Engineering, Progressive Education Society's Modern College of Engineering, Pune, IND

Corresponding authors: Vivekanand S. Jawale, vivekjawale25@gmail.com, Vikram Pandit, vikramupandit@gmail.com

Received 05/07/2025
Review began 05/13/2025
Review ended 06/03/2025
Published 06/22/2025

DOI: https://doi.org/10.7759/s44388-025-06430-7

Abstract

The present paper describes the oxidative polymerization synthesis of fibrous polyaniline, which is characterized by a number of analytical methods such as Raman analysis, Fourier-transform infrared spectroscopy, scanning electron microscopy, X-ray diffraction, and diffuse reflectance spectroscopy. The degradation of organic dyes (Aniline Blue, Crystal Violet, Rhodamine 6G, and Safranin) under exposure to visible light was used to assess the photocatalytic activity of the polyaniline. The results showed remarkable degradation efficiency, with 99.97% of Aniline Blue demineralized after 50 minutes. With a rate constant of 4.32×10^{-2} min^{-1}, the degradation kinetics exhibited a pseudo-first-order model and were noticeably higher than those of the other dyes that were examined. Polyaniline is a potential material for wastewater treatment applications because of its strong photocatalytic activity and stability. This study demonstrates polyaniline's potential as a sustainable and effective photocatalyst for environmental remediation, providing a workable alternative for the degradation of organic pollutants. The results point to Polyaniline's potential for useful implementation in a range of environmental remediation procedures.

Categories: Advanced Materials, Catalysis and Reaction Engineering, Polymer Science and Engineering
Keywords: polyaniline, photocatalysis, dye degradation, reactive oxygen species, visible-light photocatalyst

Introduction

Water contamination has become a major global issue as a result of fast industrialization, agricultural growth, and rising household waste [1-3]. Toxic pollutants found in water bodies include heavy metal ions, dyes, phenols, pesticides, and pharmaceutical residues, which have harmed both human health and environmental ecosystems [4-6]. Conventional wastewater treatment procedures frequently fail to fully remove these persistent organic pollutants [7-10]. As a result, advanced oxidation processes (AOP) [7-9] have received attention for their ability to degrade such contaminants by producing reactive radicals under a variety of light sources, including UV, visible, microwave, and solar irradiation. Among the many AOPs, heterogeneous semiconductor photocatalysis has been extensively studied as a cost-effective and environmentally benign solution to wastewater treatment [10,11].

Our research group previously reported various semiconductor photocatalysts, including TiO_2 [12], α-Fe_2O_3 [13], ZnO [14,15], MoS_2 [16], CdS [17], Fe_2O_4 [18], and others, which offer high potential for organic dye degradation, water splitting [19], and environmental cleanup. These materials were extensively explored for their chemical stability, non-toxicity, and wide range of applications [20]. Despite these advancements, semiconductor photocatalysts face challenges such as rapid electron-hole recombination, which significantly reduces their photocatalytic efficiency [21]. To overcome these limitations of traditional semiconductor photocatalysts, our group has turned to alternative materials, including conducting polymers (CPs). These CPs provide high surface area, tunable optoelectronic properties, and improved charge transport, making them useful in electronic devices like Light Emitting Diodes (LEDs), transistors, solar cells, and so on. Recently, they have been applied in environmental remediation due to their photocatalytic efficiency under visible light, aiding in pollutant degradation. Zujovic et al. optimized the degree of polymerization through π-π* stacking [22], which boosts the charge migration and photocatalytic performance.

Polyaniline is one of the most extensively studied conducting polymers due to its ease of synthesis, environmental stability, and unique electronic properties [4,22-24]. Although polyaniline has been widely applied in rechargeable batteries, organic field transistors [25], and polymer LEDs, its photocatalytic potential has remained largely unexplored. This study explores the synthesis of polyaniline via oxidative polymerization and characterizes it using various analytical techniques, including X-ray diffraction (XRD), scanning electron microscopy (SEM), Fourier-transform infrared spectroscopy (FTIR), ultraviolet (UV)-visible diffuse reflectance spectroscopy (DRS), Raman, and thermogravimetric analysis (TGA). These analyses confirmed the successful formation of polyaniline. The synthesized material was extensively used for photocatalytic activity for the degradation of organic dyes such as Aniline Blue, Crystal Violet, Rhodamine 6G, and Safranin under visible light irradiation. The results showed that polyaniline achieved

99.97% degradation of Aniline Blue within 50 minutes. The degradation followed a pseudo-first-order kinetic model, with a rate constant of 4.32×10^{-2} min^{-1}, which is fivefold higher than safranin (0.19×10^{-2}). The enhanced photocatalytic activity of polyaniline was attributed to its π-π* transition mechanism, which facilitates efficient electron transfer. We believe that the present study will open new doors for polymer and polymer composite learners for various applications.

Materials And Methods

Chemicals used for the synthesis

Aniline (C_6H_7N) (monomer), muriatic acid (HCl) (36%) (dopant and solvent), ammonium persulphate $(NH_4)_2S_2O_8$ (APS) (oxidant), and absolute ethanol are used for washing; deionized (DI) water is used as the solvent throughout the experiment; and Aniline Blue (AB), Crystal Violet (CV), Rhodamine 6G (Rh6G), and Safranin (SF) model dyes are used. All chemicals were purchased from Qualigens Thermo Fisher Scientific India Pvt. Ltd. The chemical reaction was carried out without further purification of chemicals.

Synthesis of polyaniline

Polyaniline is synthesized via chemical oxidative polymerization. Figure *1* represents a schematic representation of the synthesis of polyaniline. The polymerization reaction occurs with a 1:1 molar ratio of aniline as the monomer and APS as the oxidant [26]. In step one, aniline (1.8 mL) and APS (4.5 g) are dissolved separately in a 1 M HCl solution with constant stirring for 1 hour. In the next step, the APS solution was drop-cast into the aniline solution at 5°C, and the mixture was left to polymerize for about 2 hours with continuous stirring. At last, a dark green solid was obtained, which implies the successful synthesis of polyaniline. The synthesized product was washed with DI water and ethanol and finally dried in an oven at 80°C for 24 hours.

FIGURE 1: Schematic representation of synthesis of polyaniline through oxidative polymerization with aniline and ammonium persulphate in 1 M muratic acid as dopant in 1:1 ratio at 5°C

APS, ammonium persulphate

Characterization

The synthesized polyaniline photocatalyst was comprehensively characterized using advanced analytical techniques to elucidate its structural, optical, and morphological properties. XRD analysis was performed on a Rigaku Ultima IV diffractometer equipped with Cu Kα radiation (λ = 1.5406 Å) to determine the crystalline structure and phase purity of the material.

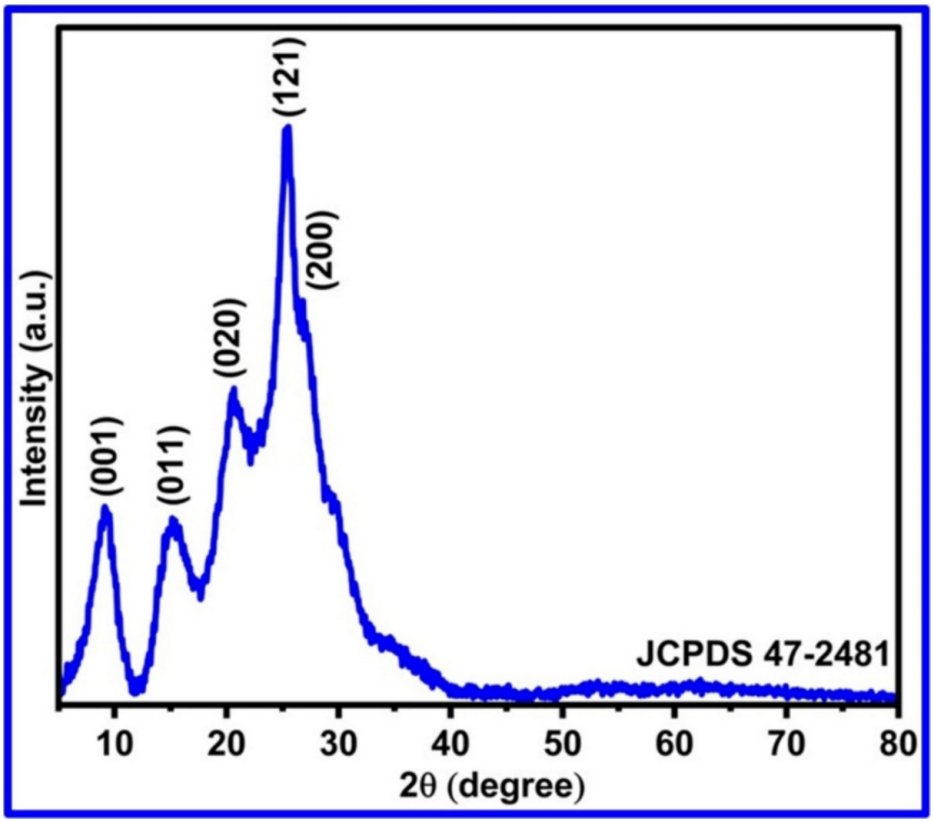

FIGURE 2: The identification and confirmation of the periodic arrangement of benzenoid and quinoid units with crystalline and semi-crystalline nature of polyaniline through X-ray diffraction

The morphological features were examined using field-emission (FE) SEM (Quanta FEG 250). Furthermore, FTIR (Shimadzu IR-Affinity-1) was employed to identify the functional groups and confirm the chemical structure of the synthesized polyaniline.

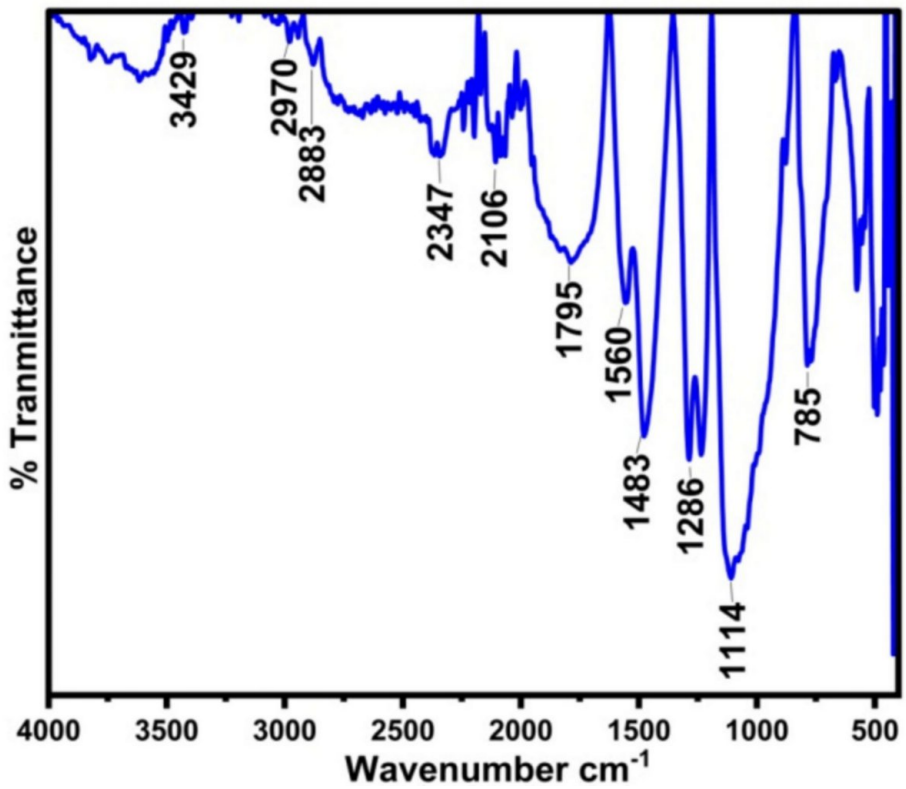

FIGURE 3: The analysis of N–H, C–H, C–N, C=C, C=N functional groups in polyaniline through FTIR spectra

FTIR, Fourier-transform infrared spectroscopy

UV-visible DRS was conducted using a Shimadzu UV-3600 spectrophotometer to assess the optical absorption properties and identify the bandgap energy.

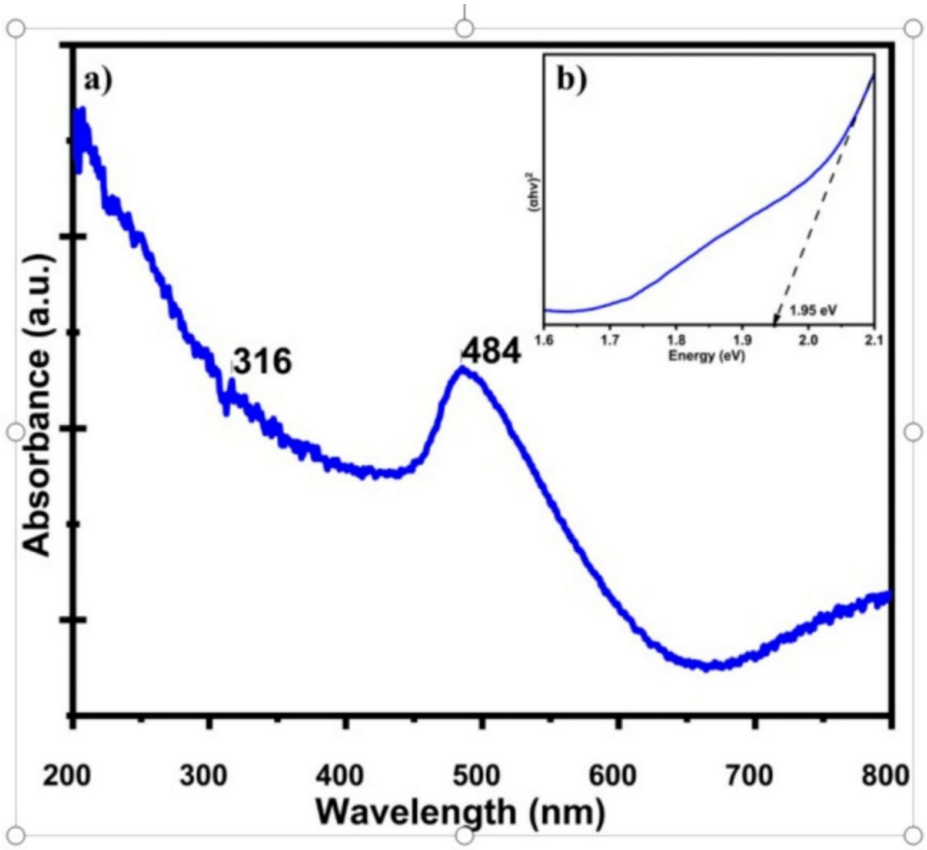

FIGURE 4: (a) UV-vis absorption spectrum of polyaniline, (b) Tau plot for estimated band gap (αhv)2 versus bandgap energy (Eg)

UV, ultraviolet

These characterization techniques collectively provided a detailed understanding of the material's physicochemical properties, facilitating the correlation between structure and photocatalytic performance.

Results

The XRD pattern of polyaniline observed in Figure *2* shows a semi-crystalline structure, characterized by a combination of broad amorphous halos and distinct crystalline peaks. The diffractogram shows a strong peak in the 2θ range of 5° to 30°, indicating good agreement in the polymer matrix. The crystallinity arises from the periodic arrangement of benzenoid and quinoid units in the polyaniline backbone. The most prominent diffraction peaks appear at 2θ ≈ 9.27° (001), 15.33° (020), 20.38° (200), and 25.41° (121), corresponding to interplanar spacings of 4.366 Å and 3.520 Å, respectively [27,28]. The peak at 20.38° is particularly significant, as it represents the inter-chain distance between benzene rings in adjacent polyaniline chains, while the reflection at 25.41° is attributed to the parallel periodicity of polymer chains, confirming a partially ordered structure.

Figure *3* explains that the FTIR spectrum of polyaniline exhibits characteristic vibrational modes corresponding to its molecular structure (Table *1*), recorded at room temperature (27°C) from 4000 to 400 cm^{-1}. An absorption band at 3429 cm^{-1} is attributed to the N-H stretching vibration of amine groups, while peaks at 2970 cm^{-1} and 2883 cm^{-1} arise from aromatic C-H stretching [24,29]. The quinoid ring stretching vibrations appear at 1795 cm^{-1}, confirming the oxidized form, whereas the benzenoid ring stretching is observed at 1560 cm^{-1}, indicative of the reduced structure. The C-N stretching vibration at 1286 cm^{-1} signifies protonation in the doped state, while the in-plane C-H bending at 1114 cm^{-1} reflects the conducting polymer synthesis. Additionally, the 785 cm^{-1} band corresponds to out-of-plane C-H vibrations in a 1,4-disubstituted aromatic ring, confirming the para-linked polymer chain. The coexistence of quinoid and benzenoid units verifies the successful synthesis of polyaniline.

Frequency Range (cm^{-1})	Functional Group/Structure	Mode of Vibration	Remarks
3429	N–H	Stretching	Amine group
2970, 2883	C–H (aromatic)	Stretching (asymmetric/symmetric)	Aromatic ring CH vibrations
1795	C=N / C=C (quinoid ring)	Stretching	Quinoid structure (oxidized form)
1560	C=C (benzenoid ring)	Stretching	Benzenoid structure (reduced form)
1494–1357	C–C (aromatic ring)	Stretching	Benzene ring backbone
1286	C–N (benzenoid/quinoid)	Stretching	Protonated amine (conducting state)
1114	C–H (in-plane bending)	Bending	Protonated polyaniline (polaronic structure)
1109–1041	Quinoid unit (N=Q=N)	Deformation	Conducting emeraldine salt form
785	C–H (aromatic, 1,4-disubstituted)	Out-of-plane bending	Para-substituted benzene ring

TABLE 1: Characteristic FTIR absorption bands, corresponding functional groups/structures, vibrational modes, and analytical remarks for polyaniline

FTIR, Fourier-transform infrared spectroscopy

Figure *4a* shows the UV-visible absorption spectrum recorded between 200 and 800 nm, which reveals three distinct absorption features. The first absorption band appears at 316 nm, corresponding to the π-π* transition of benzenoid segments. Most notably, a prominent peak observed at approximately 490 nm is attributed to the n-π* transition between the Highest Occupied Molecular Orbital (HOMO) of benzenoid rings and Lowest Unoccupied Molecular Orbital (LUMO) of quinoid rings, which is crucial for polyaniline electrical conductivity [23,30].

Additionally, polyaniline shows a broad absorption above the 700 nm region, arising from the π-π* polaron transition that indicates charge delocalization in quinoid units. These longer wavelength absorptions (650-800 nm) signify charge-transfer excitations and polaron formation, which are essential for polyaniline's conductive properties. The optical bandgap energy of polyaniline was investigated using UV-visible DRS, which confirms the semiconductor behavior. The Kubelka-Munk method was employed to analyze the diffuse reflectance, where the

Kubelka-Munk function, F(R), was derived from the reflectance (R) using the relation

$$F(R) = (1 - R)^2/2R \quad \text{.....(1)}$$

The bandgap energy was determined by plotting versus photon energy (hv), where α represents the absorption coefficient. The plot of $(\alpha hv)^2$ versus bandgap energy (E_g) was estimated by extrapolating the linear portion of the curve to the energy axis. The analysis revealed a bandgap of 1.95 eV for the polyaniline, as illustrated in Figure *4b*, reported bandgap energies for polyaniline in its conductive form, suggesting that the synthesized nanoparticles retain the intrinsic semiconducting properties of polyaniline. The obtained bandgap indicates that nanoparticles are suitable for optoelectronic engineering applications, including solar cells and organic semiconductors, highlighting their potential in photoelectrochemical and photocatalytic applications.

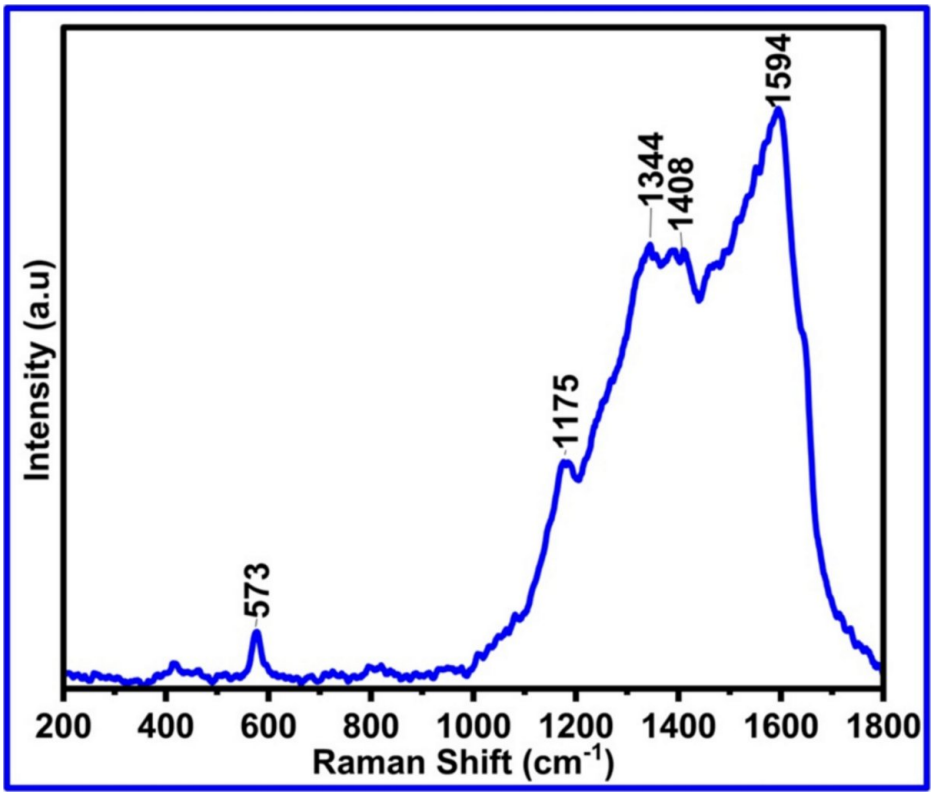

FIGURE 5: Raman spectrum for analysis of polymeric structure, C-H bending vibrations, C-N^{+}• stretching vibration of the polaronic structure in polyaniline

The Raman spectrum of the synthesized polyaniline, presented in Figure *5*, exhibits several characteristic vibrational modes in the spectral range of 1000-1800 cm^{-1}, which confirms the polymeric structure. The observed peaks at 1175 cm^{-1} correspond to C-H bending vibrations in the benzenoid and quinoid rings, which are fundamental structural units of polyaniline. A prominent peak appears at 1344 cm^{-1}, assigned to the C-N^{+}• stretching vibration of the polaronic structure.

Further analysis reveals two distinct bands at higher wavenumbers: the peak at 1408 cm^{-1} represents C=N stretching in quinoid units, while the 1594 cm^{-1} feature corresponds to C=C stretching vibrations in the quinoid rings. These characteristic vibrational modes collectively confirm the presence of both benzenoid and quinoid structures in the polyaniline, which facilitate the conductivity. The absence of extraneous peaks in the spectrum indicates the high purity of the synthesized material, consistent with structural characterization results from Energy-dispersive X-ray spectroscopy (EDS) and XRD analysis.

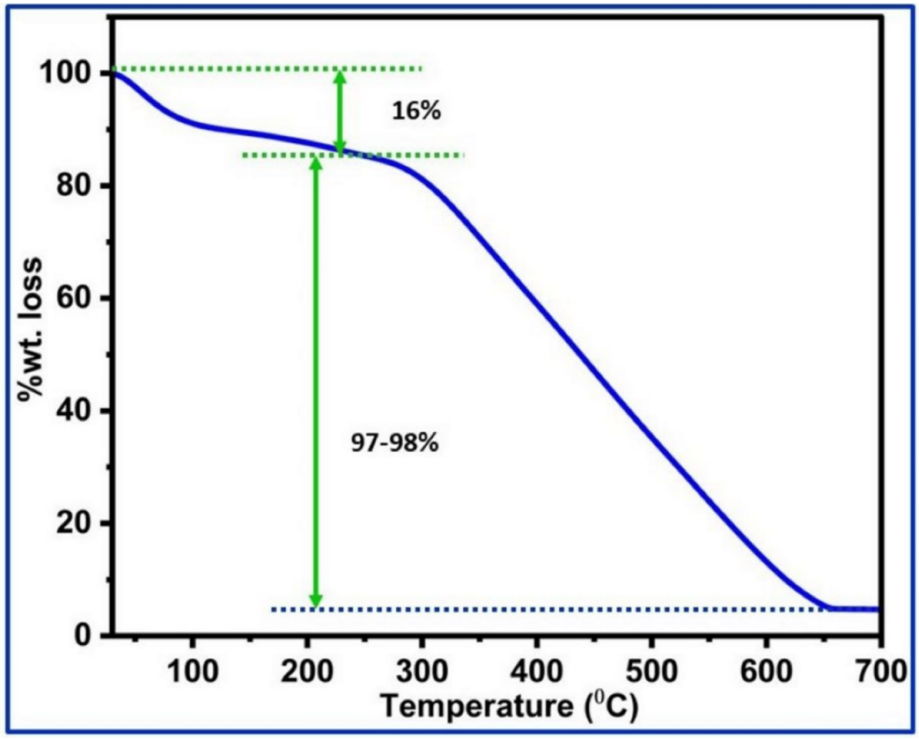

FIGURE 6: Thermogravimetric analysis (TGA) of polyaniline demonstrating thermal stability

TGA data presented in Figure *6* and the accompanying description show the thermal degradation behavior of pure polyaniline. An initial weight loss of approximately 16% occurs at 235°C, attributed predominantly to the evaporation of absorbed moisture within the polymer matrix. Subsequently, it undergoes extensive thermal decomposition, culminating in a near-complete mass loss of 97-98% by 700°C. This significant mass loss at high temperature indicates the inherent thermal stability of the pure polyaniline.

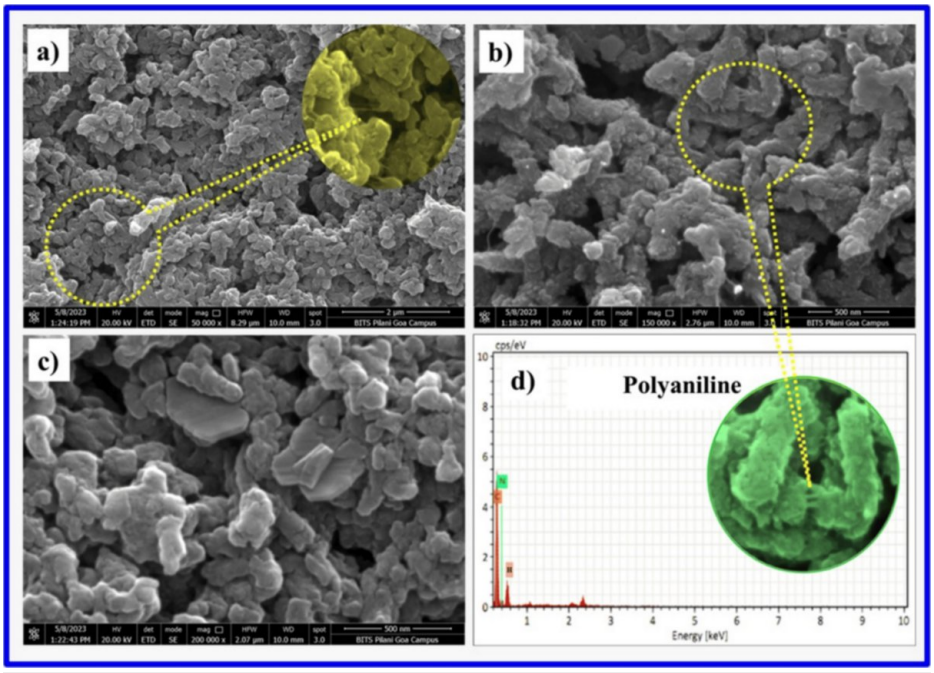

FIGURE 7: (a) Low magnification level Field Emission Scanning Electron Microscopic (FESEM) analysis of polyaniline nanoparticles, (b and c) higher magnification level FESEM image of polymeric linkage in polyaniline. (d) Energy-dispersive X-ray spectroscopy (EDS) analysis of the polyaniline shows the presence of carbon (C), Nitrogen (N), and Hydrogen (H) with its elemental composition

Figure 7a to 7c explains the SEM analysis of the synthesized polyaniline nanoparticles, which provides valuable information about their surface morphology and structural characteristics. The low-magnification SEM image (Figure 7a) reveals a uniform distribution of nanoparticles across the surface, indicating a controlled polymer synthesis process. Figure 7a insights highlight the polymeric linkage in the synthesis. Figure 7b leads to an increase in the surface area, which enhances the number of active sites available for catalytic reactions. Thus, the observed morphology of polyaniline nanoparticles directly contributes to improved photocatalytic performance, especially in the degradation of organic dyes.

Sr. No.	Element	Weight%	Atomic%
1	C	64	73.3
2	N	15.4	15.1
3	H	7.1	6.1

TABLE 2: Elemental composition (Weight% and Atomic%) of polyaniline determined by energy-dispersive X-ray spectroscopy (EDS) analysis

EDS analysis of the polyaniline shown in Figure 7d confirms the presence of key constituent elements, including carbon (C), nitrogen (N), and hydrogen (H), with no detectable impurities. The quantitative EDS results revealed the following elemental composition: 72.22% C, 12.30% N, and 15.78% H. These findings are recorded in Table 2, which are consistent with the expected chemical structure of polyaniline, verifying its successful synthesis. The absence of additional elemental peaks further confirms the purity of the synthesized polyaniline nanoparticles, supporting their suitability for further functional applications. At higher magnification, the SEM image shows that the nanoparticles are predominantly spherical in shape and tend to agglomerate, forming clusters with an average particle size ranging from 20 to 30 nm (Figure 8), which is aligned with XRD analysis. Thus, the observed morphology of polyaniline nanoparticles directly contributes to improved photocatalytic performance, especially in the degradation of organic

dyes.

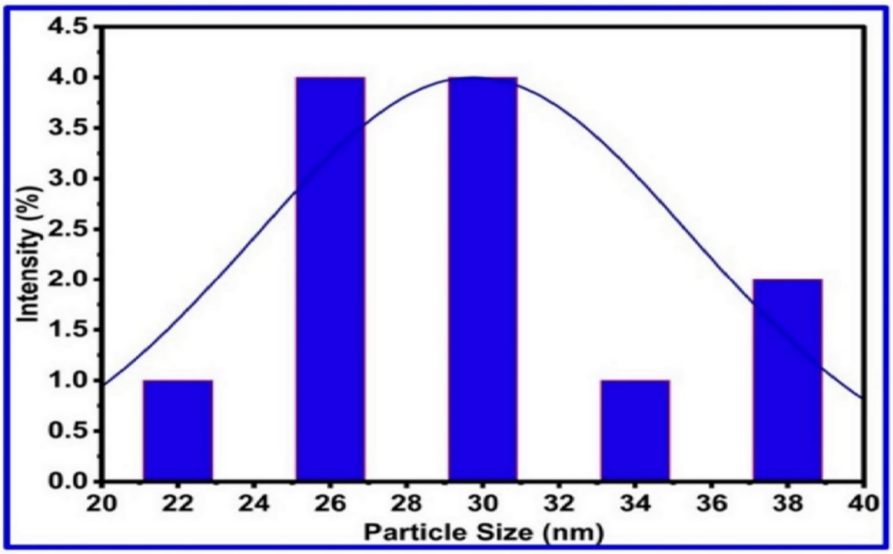

FIGURE 8: Histogram analysis of particle size distribution

Discussion

The photocatalytic performance of polyaniline was evaluated using various dyes (Table 3), including Aniline Blue (AB), Crystal Violet (CV), Rhodamine 6G (Rh6G), and Safranin (SF).

Dye	Molecular Formula	Degradation Efficiency (%)	IUPAC Name	Physical Characters			
				Mwt	Color	Solubility (mg L−1) in water	Absorption maxima (λmax)
Rhodamine 6G	C28H31N2O3Cl	34.75	9-[2-(Ethoxycarbonyl)phenyl]-N-ethyl-6- (ethylamino)-2,7-dimethyl-3H-xanthen-3-iminium chloride	479.02	Red	4 × 103	530
Crystal Violet	C25H30ClN3	80.69	Tris(4- (dimethylamino)phenyl)methylium chloride	407.99	Blue Violet	4 × 103	590
Safranin	C20H19N +Cl - 4	11.6	3,7-dimethyl-10-phenylphenazin-10- ium-2,8-diamine; chloride	350.85	Red	1 × 103	476 and 493
Aniline Blue	C32H25N3Na2O9S3	99.97	disodium 2-{[4-({4-[(2- sulfonatophenyl)amino]phenyl}({4-[(2-sulfonatophenyl)imino]cyclohexa-2,5- dien-1-ylidene})methyl)phenyl]amino}benzene- 1-sulfonate	737.73	Blue	1 × 103	595-610

TABLE 3: Synthetic dyes with their key chemical properties (molecular formula, structure, and IUPAC name) and physical characteristics, including molecular weight (Mwt), color, aqueous solubility, and absorption maxima (λmax)

The experiments were conducted by dispersing 50 mg of polyaniline in 100 mL of dye solution (10 ppm) under sunlight irradiation. Prior to light exposure, the mixture was stirred in the dark to establish adsorption-desorption equilibrium, ensuring optimal dye adsorption onto the polyaniline surface. The degradation process was monitored via UV-vis spectrophotometry, where the decrease in absorbance

indicated demineralization.

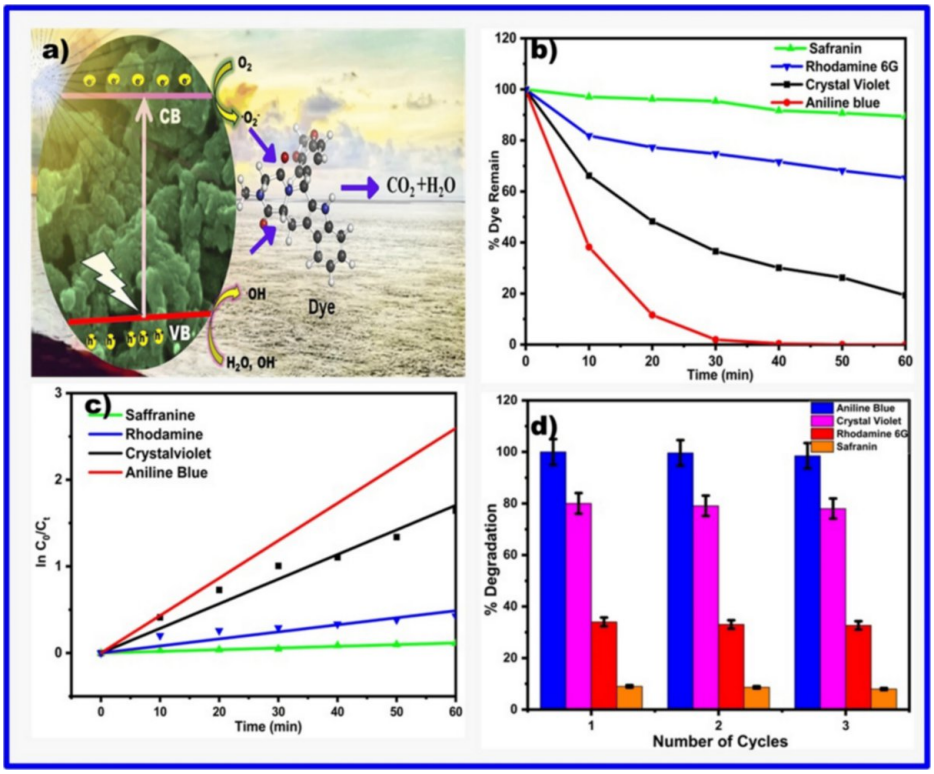

FIGURE 9: (a) Photocatalysis mechanism, (b) extent of decomposition of the AB, CV, RH6G, and SF dyes with respect to time intervals over polyaniline under natural sunlight irradiation (catalyst concentration: 0.5 mg/mL; initial concentration of dyes: 10ppm). (c) Comparison of the rate constants of AB, CV, RH6G, and SF dyes in the presence of polyaniline under natural sunlight irradiations (catalyst concentration: 0.5 mg/mL; initial concentration of dyes: 10ppm). (d) Multiple recycle studies for the dye degradation of AB, CV, RH6G, and SF dyes

AB, Aniline Blue; CV, Crystal Violet; RH6G, Rhodamine 6G; SF, Safranin

Figure *9a* proposes the photocatalytic efficiency of polyaniline and the degradation mechanism toward dyes, particularly AB dye. It absorbs sunlight, which promotes electrons (e^-) from the HOMO to the LUMO, leaving holes (h^+) in the valence band [31,32]. The excited e^- reacts with dissolved O_2 to form superoxide radicals ($\bullet O_2^-$). The h^+ reacts with H_2O/OH^- to produce hydroxyl radicals (OH^-). The generated ROS ($\bullet O_2^-$. OH^-) attack the dye molecules and facilitate mineralization dye (CO_2, H_2O).

Figure *9b* to 9c observed remarkable photocatalytic efficiency, particularly for AB, achieving 99.97% degradation within 50 minutes, with a rate of 4.32×10^{-2} min^{-1}. In contrast, SF showed a lower degradation efficiency with a rate constant of 0.19×10^{-2} min^{-1}, attributed to its structural stability. Among the tested dyes (Figure *10a*-d), the degradation rates are documented in Table *4*, following the order AB > CV > Rh6G > SF.

Dye	Rate of Degradation (min^{-1})	Standard Error
Aniline Blue	4.32×10^{-2}	0.0253
Crystal Violet	2.84×10^{-2}	0.0012
Rhodamine 6G	0.81×10^{-2}	0.0007
Safranin	0.19×10^{-2}	0.0000

TABLE 4: Photocatalytic degradation rates and standard errors of various dyes mediated by polyaniline under sunlight

The reusability potential of polyaniline for the photocatalytic degradation of AB, CV, Rh6G, and SF was evaluated over three consecutive cycles, with the catalyst recovered via centrifugation, washed with DI water, and dried after each use. Polyaniline exhibited excellent stability, maintaining high degradation efficiency across cycles, as evidenced by the minimal decline in performance of dyes over three cycles attributed to sustained reactive oxygen species (ROS) generation, particularly •OH radicals. Post-recycling XRD analyses confirmed polyaniline's structural integrity, as shown in Figure *11*, with no significant changes in crystal structure or functional groups, highlighting its robustness and suitability for repeated use in dye degradation applications. Further optimization could enhance its efficiency, but the results underscore polyaniline's potential as a reusable photocatalyst for wastewater treatment.

Conclusions

In a nutshell, fibrous polyaniline was effectively synthesized and described in this study, and it showed impressive photocatalytic activity when exposed to visible light. The material may find use in wastewater treatment due to its high degradation efficiency, especially for Aniline Blue. With 99.97% of Aniline Blue destroyed after 50 minutes, the results showed remarkable degradation efficiency. With a rate constant of 4.32×10^{-2} min^{-1}, the degradation kinetics exhibited a pseudo-first-order model and were noticeably higher than those of the other dyes that were examined. Mechanistic studies elucidated that visible light excitation generates electron-hole pairs in polyaniline, which subsequently produce ROS, such as superoxide anion radicals ($•O_2^-$) and hydroxyl radicals (•OH). These ROS drive the mineralization of AB into non-toxic byproducts. Recycling experiments highlighted polyaniline stability, retaining 98.5% degradation efficiency after three consecutive cycles, affirming its potential for sustainable reuse. In conclusion, we report the successful synthesis of environmentally stabilized polyaniline, which emerges as a robust, recyclable photocatalyst with high efficacy for water purification. Future research should explore polyaniline-based composites to further enhance performance and stability, advancing scalable solutions for environmental remediation, energy storage (supercapacitors, batteries), sensors, corrosion-resistant coatings, biomedical devices (drug delivery, tissue engineering), and environmental remediation (adsorbents, EMI shielding). Their tunable conductivity, redox activity, and synergy with materials like graphene or metal oxides enable innovations in sustainable technologies and smart systems.

Appendices

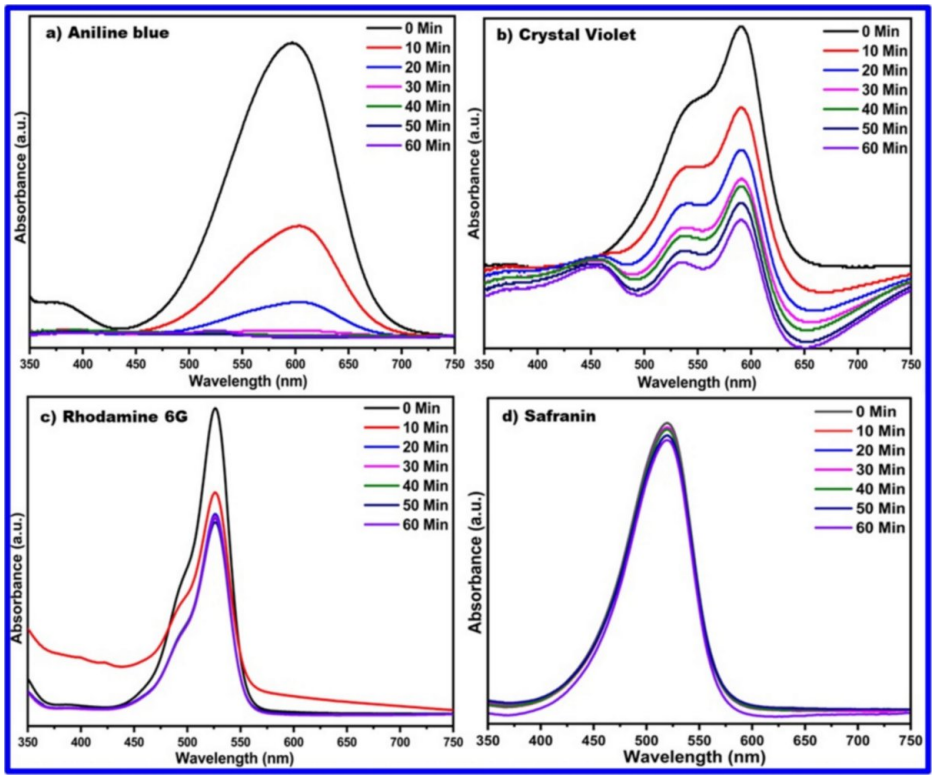

FIGURE 10: Photocatalytic activity of polyaniline for degradation of Aniline Blue, Crystal Violet, Rhodamine 6G, Safranin (catalyst concentration: 0.5 mg/mL; initial concentration of dyes: 10ppm)

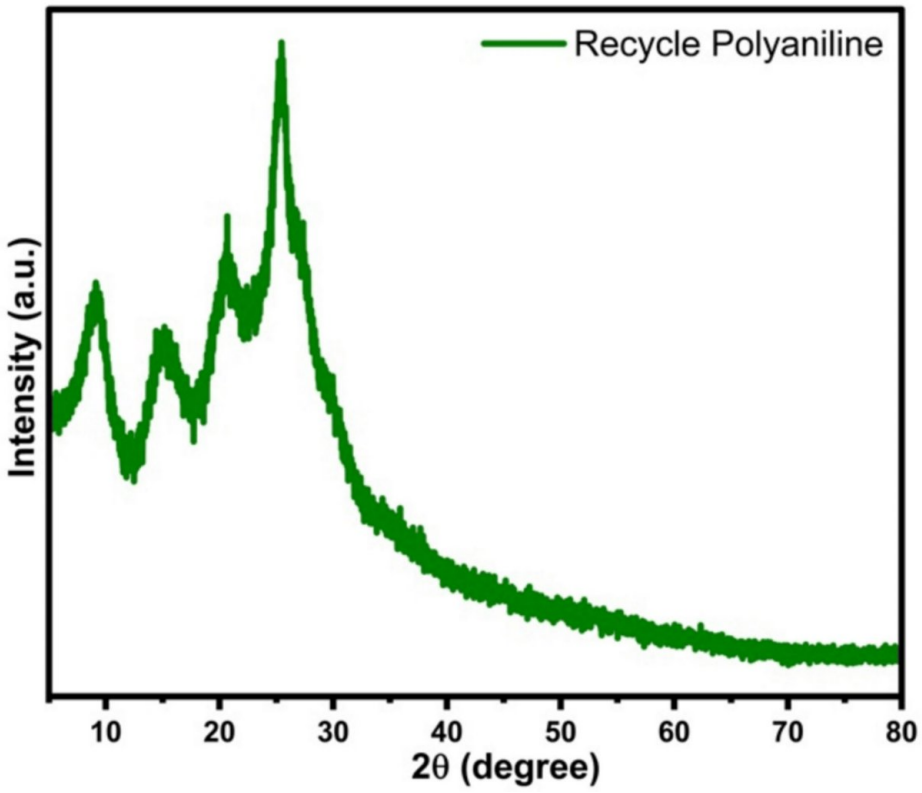

FIGURE 11: XRD of polyaniline after Aniline Blue dye degradation

XRD, X-ray Diffraction

Additional Information

Author Contributions

All authors have reviewed the final version to be published and agreed to be accountable for all aspects of the work.

Concept and design: Vikram Pandit, Vivekanand S. Jawale, Bhagwan Daphal, Vrishali Edlabadkar

Acquisition, analysis, or interpretation of data: Vikram Pandit, Vivekanand S. Jawale, Bhagwan Daphal, Vrishali Edlabadkar

Drafting of the manuscript: Vikram Pandit, Vivekanand S. Jawale, Bhagwan Daphal, Vrishali Edlabadkar

Critical review of the manuscript for important intellectual content: Vikram Pandit, Vivekanand S. Jawale, Bhagwan Daphal, Vrishali Edlabadkar

Supervision: Vikram Pandit, Vivekanand S. Jawale, Bhagwan Daphal, Vrishali Edlabadkar

Disclosures

Human subjects: All authors have confirmed that this study did not involve human participants or tissue. **Animal subjects:** All authors have confirmed that this study did not involve animal subjects or tissue. **Conflicts of interest:** In compliance with the ICMJE uniform disclosure form, all authors declare the following: **Payment/services info:** All authors have declared that no financial support was received from any organization for the submitted work. **Financial relationships:** All authors have declared that they have no financial relationships at present or within the previous three years with any organizations that might have an interest in the submitted work. **Other relationships:** All authors have declared that there are no other relationships or activities that could appear to have influenced the submitted work.

Acknowledgements

Authors would like to thank the principal of H. V. Desai College and Modern College of Engineering, Pune,

for their lab facilities. Authors would also like to thank Dr. S. Satpal for characterization and Mr. Omkar Malusare and Mr. G. Jadhav for helping with photocatalytic experiments data interpretation. BDD would also like to thank Savitribai Phule Pune University (SPPU) for providing the opportunity to conduct research work.

References

1. Ashbolt NJ: Microbial contamination of drinking water and disease outcomes in developing regions. Toxicology. 2004, 198:229-38. 10.1016/j.tox.2004.01.030
2. Pandey PK, Kass PH, Soupir ML, Biswas S, Singh VP: Contamination of water resources by pathogenic bacteria. AMB Express. 2014, 4:51. 10.1186/s13568-014-0051-x
3. Nemiwal M, Zhang TC, Kumar D: Recent progress in g-C3N4, TiO2 and ZnO based photocatalysts for dye degradation: Strategies to improve photocatalytic activity. The Science of The Total Environment. 2021, 767:144896. 10.1016/j.scitotenv.2020.144896
4. Zia J, Riaz U: Photocatalytic degradation of water pollutants using conducting polymer-based nanohybrids: A review on recent trends and future prospects. Journal of Molecular Liquids. 2021, 340:117162. 10.1016/j.molliq.2021.117162
5. Zhang T, Wang X, Zhang X: Recent progress in TiO2-mediated solar photocatalysis for industrial wastewater treatment. International Journal of Photoenergy. 2014, 2014:607954. 10.1155/2014/607954
6. Konstantinou IK, Albanis TA: TiO2-assisted photocatalytic degradation of azo dyes in aqueous solution: kinetic and mechanistic investigations. Applied Catalysis B Environment and Energy. 2004, 49:1-14. 10.1016/j.apcatb.2003.11.010
7. Rana A, Sonu S, Sudhaik A, et al.: Tailoring dual S-Scheme based g-C3N4/ZnO/TiO2 ternary photocatalytic system immobilized on floating cork for environmental remediation. Journal of the Taiwan Institute of Chemical Engineers. 2025, 168:105914. 10.1016/j.jtice.2024.105914
8. Piaskowski K, Świderska-Dąbrowska R, Zarzycki PK: Dye removal from water and wastewater using various physical, chemical, and biological processes. Journal of AOAC International. 2018, 101:1371-384. 10.5740/jaoacint.18-0051
9. Turkten N, Karatas Y, Bekbolet M: Preparation of PANI modified ZnO composites via different methods: structural, morphological and photocatalytic properties. Water. 2021, 13:1025. 10.3390/w13081025
10. González-vázquez MY, Carrillo-martínez CJ, Pinedo-Escobar JA, et al.: Photocatalytic degradation of methyl orange and metoprolol by novel ternary photocatalyst TiO2-ZnO/g-C3N4 under UV and visible light . Prerpints.org. 2024, 0-15. 10.20944/preprints202410.2481.v1
11. Das BR, Jena S, Dhal JP: Ag doped α-Fe2O3 nanoparticles: Synthesis, characterization and application as heterogeneous photocatalyst for removal of organic dye from aqueous media without any oxidizing agents. Journal of the Indian Chemical Society. 2021, 98:100214. 10.1016/j.jics.2021.100214
12. Pandit V, Arbuj S, Hawaldar R, et al.: In situ preparation of a novel organo-inorganic 6,13-pentacenequinone-TiO2 coupled semiconductor nanosystem: a new visible light active photocatalyst for hydrogen generation. Journal of Materials Chemistry A. 2015, 3:4338-344. 10.1039/c4ta06606e
13. Pandit VRU, Jadhav GKP, Jawale VMS, et al.: Synthesis and characterization of micro-/nano-α-Fe2O3 for photocatalytic dye degradation. RSC Advances. 2024, 14:29099-9105. 10.1039/d4ra04575k
14. Jawale V, Al-fahdawi A, Salve S, et al.: 6,13-pentacenequinone/zinc oxide nanocomposites for organic dye degradation. Materials Today Proceedings. 2022, 52:17-20. 10.1016/j.matpr.2021.10.098
15. Jawale V, Gugale G, Chaskar M, et al.: Two- and three-dimensional zinc oxide nanostructures and its photocatalytic dye degradation performance study. Journal of Materials Research. 2021, 36:1573-583. 10.1557/s43578-021-00174-w
16. Gawari D, Pandit V, Jawale N, Kamble P: Layered MoS2 for photocatalytic dye degradation. Materials Today Proceedings. 2022, 53:10-14. 10.1016/j.matpr.2021.12.194
17. Pandit VU, Arbuj SS, Hawaldar RR, et al.: Hierarchical CdS nanostructure by Lawesson's reagent and its enhanced photocatalytic hydrogen production. RSC Advances. 2015, 5:13715-3721. 10.1039/c4ra15138k
18. Shinde CS, Sali ND, Dhawale SK, Dhanwate VN, Jawale V: Influence of Co2+ ions on structural, optical, and magnetic properties of inverse spinel lithium ferrite nanoparticles. Cureus Journal Of Engineering. 2025, 1-14. 10.7759/s44388-024-02854-9
19. Pandit VRU: Hydrogen as a clean energy source. Alternative Energies and Efficiency Evaluation. 2022. 326. 10.5772/intechopen.101536
20. Satpal SB, Athawale AA: Synthesis of ZnO and Nd doped ZnO polyscales for removal of rhodamine 6G dye under UV light irradiation. Materials Research Express. 2018, 5:1-13. 10.1088/2053-1591/aad26c
21. Dhawale SK, Sarvalkar PD, Shinde CS, Prasad NR, Garadkar KM, Sharma KKK, Ramteke AA: Studies on photocatalytic and antioxidant efficacy of Ag-embedded ZnO nnocomposites. ACS Omega. 2025, 10:11948-1960. 10.1021/acsomega.4c08896
22. Zujovic ZD, Laslau C, Bowmaker GA, Kilmartin PA, Webber AL, Brown SP, Travas-Sejdic J: Role of aniline oligomeric nanosheets in the formation of polyaniline nanotubes. Macromolecules. 2010, 43:662-70. 10.1021/ma902109r
23. Rafiq S, Lovely MA, Mim SR, Islam MS, Hasan M, Billah MM: Structure controlled enhanced photocatalytic activity of polyaniline (PANI). Heliyon. 2025, 11:e42888. 10.1016/j.heliyon.2025.e42888
24. Gedanken A: Photocatalytic degradation of organic dyes and antimicrobial activities by polyaniline - nitrogen-doped carbon dot nanocomposite. Nanomaterials . 2021, 11:1128.
25. Bhadra S, Khastgir D, Singha NK, Lee JH: Progress in preparation, processing and applications of polyaniline. Progress in Polymer Science. 2009, 34:783-810. 10.1016/j.progpolymsci.2009.04.003
26. Paul SJ, Gupta BK, Chandra P: Probing the electrical and dielectric properties of polyaniline multi-walled carbon nanotubes nanocomposites doped in different protonic acids. Polymer Bulletin. 2020, 78:5667-683. 10.1007/s00289-020-03399-7
27. Schöntag J, Ströbele M, Schubert H, Bettinger HF: Nucleophilic addition of bulky aryl substituents to pentacene-6,13-quinone. European Journal of Organic Chemistry. 2024, 27:e202301161. 10.1002/ejoc.202301161

28. Feng TZ, Lv Q, Lv ZJ, Xu CF, Jiang JH, Wang XD: In-plane hierarchical assembly of two-dimensional molecular crystals toward on-chip multimode optical waveguides. Science Advances. 2025, 11:eadt0938. 10.1126/sciadv.adt0938
29. Zor S, Budak B: Investigation of the effect of PAn and PAn/ZnO photocatalysts on 100% degradation of Congo red under UV visible light irradiation and lightless environment. Turkish Journal of Chemistry. 2020, 44:486-501. 10.3906/kim-1907-30
30. Pal R, Goyal SL, Rawal I, Gupta AK, Ruchi: Efficient energy storage performance of electrochemical supercapacitors based on polyaniline/graphene nanocomposite electrodes. Journal of Physics and Chemistry of Solids. 2021, 154:110057. 10.1016/j.jpcs.2021.110057
31. Chou SY, Chen CC, Dai YM, Lin JH, Lee WW: Novel synthesis of bismuth oxyiodide/graphitic carbon nitride nanocomposites with enhanced visible-light photocatalytic activity. RSC Advances. 2016, 6:33478-3491. 10.1039/c5ra28024a
32. Pandit VU, Daphal BD, Jadhav GP: Effect of Fe doping on dye degradation of calcium titanate. Cureus Journal of Engineering. 2025, 10.7759/s44388-025-03407-4